J Mater Sci (2009) 44:1734–1740
DOI 10.1007/s10853-008-3084-1

Pt effects in γ-Ni(Al)/α-Al_2O_3 adhesion

Yong Jiang · John R. Smith

Received: 10 June 2008 / Accepted: 24 October 2008 / Published online: 23 November 2008

Abstract We present a systematic first-principles density-functional theory (DFT) study of the effects of Pt on the adhesion of the γ-Ni(Al)/α-Al_2O_3 interface, in a close comparison with those of Hf and S. Both the thermodynamically preferred Al-rich and the stoichiometric interfaces are considered. S is found to segregate to and substantially weaken both interfaces. Hf can pin S in bulk γ-Ni even at temperatures as high as 1,600 K, effectively inhibiting S segregation, while Pt cannot, due to phonon effects. For the stronger, Al-rich interface, both Hf and Pt have larger heats of segregation than S, inhibiting S segregation through preferential segregation. For the weaker, stoichiometric interface, Hf can significantly strengthen its adhesion to be as large as that of the Al-rich interface, and also inhibit S segregation through preferential segregation. Pt, as a contrast, can neither inhibit S segregation nor directly enhance the interface bonding.

Introduction

Multilayer thermal barrier coatings (TBCs) are present in high-temperature turbines for propulsion and power generation, and offer remarkable improvement in performance and longevity for various load-bearing, hot section components [1]. A typical TBC comprises three primary layers: the outer stabilized zirconia imparts thermal protection, while the Ni-alloy bond coat (BC) affords oxidation protection through the formation of an intermediate layer of thermally gown oxide (TGO), as well as mitigation of mismatch strain [1–3]. Figure 1 shows cross sections of an actual tri-layer thermal barrier system in these applications. It is critical that the Ni-alloy BC contains sufficient Al so as to preferentially form the protective α-Al_2O_3 (TGO) upon oxidation. For a two-phase BC alloy (consisting of γ-Ni(Al)/β-NiAl or γ-Ni(Al)/γ'-Ni_3Al phases), the growth of α-Al_2O_3 depletes β or γ', which can leave a continuous single-phase layer of γ-Ni(Al) adjacent to the interface (see Fig. 1). To sustain oxidation protection, the α-Al_2O_3 must remain in effective bonding with the alloy during thermal cycling: otherwise, delamination occurs at the interface, causing the Al_2O_3 protective layer to spall. Earlier experiments have suggested that delamination is enhanced by impurities (such as S) [4–8], but can be alleviated by certain reactive-element (RE) dopants (such as Hf, Y, and Zr) and noble-metal alloying elements (such as Pt) [9–14]. The beneficial influence of RE-dopants has been hypothesized to be attributed to scavenging of the S in the bulk Ni alloy, preventing segregation to the interface, and/or the direct promotion of interfacial bonding. The fundamentals governing these mechanisms remain unclear. It is still a question whether Pt could play the same roles as RE-dopants. That aside, it is also suggested that the Pt benefits might be related to the formation and growth kinetics of the oxide, by reducing interfacial void formation [15–19], promoting the selective formation of the stable and protective α-Al_2O_3 phase [19–24], and/or the relaxation of growth stresses in the oxide [25]. Beyond the effects exerted by doping/alloying and impurity elements, the interface adhesion is also sensitive to the atomic termination (stoichiometry) of the α-Al_2O_3 in contact with the

Y. Jiang (✉) · J. R. Smith
Materials Department, University of California, Santa Barbara, CA 93106, USA
e-mail: yjiang@engr.ucsb.edu

Y. Jiang
Chemical and Mechanical Engineering Department, University of California, Santa Barbara, CA 93106, USA

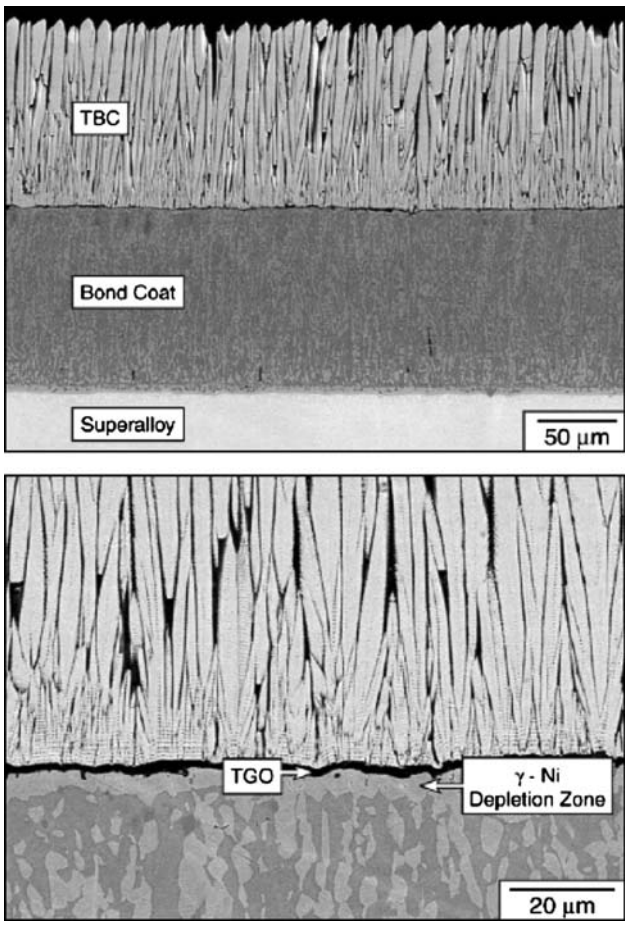

Fig. 1 Cross sections of an actual tri-layer thermal barrier system indicating the functionalities of each of the layers [3]

Ni-alloy [26]. The stoichiometric interface is the weakest, with the Al-rich and O-rich interfaces exhibiting stronger binding. The interfacial stoichiometry, in turn, depends on the chemical activity of Al in the Ni-alloy (a_{Al}) during oxidation [26–30]. All these factors may exert combined and complex effects on the adhesion, making it prohibitive to rely solely on experimental studies.

First-principles calculations have emerged as an indispensable tool that allows new valuable insights into many fundamental aspects of this important interface [26–32]. In this article, we report a systematic assessment of the adhesion of the γ-Ni(Al)/α-Al_2O_3 interface achieved from first-principles. Of particular interest here is the potential for noble-metal Pt to affect adhesion of this interface. The ensuing article is organized into the following parts: (i) the methodology and the computational approach are summarized, (ii) clean (impurity free) interface structures and corresponding interfacial strengths are determined, (iii) segregation sites and tendencies at the interface are determined and their effects on adhesion are quantified, and (iv) gettering of impurities in bulk γ-Ni by additives is examined.

Methodology

Our basic strategy is to isolate and follow the factors that might potentially affect adhesion by noble-metal Pt and to quantify their individual and combined effects via ab initio energetics calculations. To realize this strategy, we have performed the following first-principles based studies on Pt effects and compared them with those of Hf and S.

(i) DFT calculations [29] of the Al activity, a_{Al}, in bulk γ-Ni(Al) as a function of the Al concentration, x_{Al}, and the temperature, T. With the assumption of thermodynamic equilibrium between bulk γ-Ni(Al) and the γ-Ni(Al)/α-Al_2O_3 interface, the interfacial phase or stoichiometry is a function of T and a_{Al}.

(ii) Determination of the γ-Ni(Al)(111)/α-Al_2O_3(0001) interfacial phase diagram for all relevant T and a_{Al}. This interface orientation is chosen according to high resolution transmission electron microscopy (HRTEM) results for Cu/α-Al_2O_3 [33]. The equilibrium interfacial structure (stoichiometry), and corresponding adhesion strength can be determined for a given x_{Al} and T by simply mapping the calculated a_{Al} onto the corresponding phase diagram [30].

(iii) Calculations of heats of segregation (ΔG_{seg}) of Pt from bulk γ-Ni to the relevant interfacial phase.

(iv) Computation of adhesion strengths in terms of the work of separation, W_{sep}, for clean and segregant-containing interfaces: W_{sep} is defined as the difference in the enthalpy between that of the fully separated interface and that of the equilibrium, bonded interface divided by the interfacial cross-sectional area.

(v) Computation of the interactions between Pt and S in bulk γ-Ni in order to determine the likelihood of gettering S in the bulk γ-Ni and thereby inhibiting S segregation to the interface.

The electronic calculations are performed using the DFT code VASP [34, 35] within the generalized gradient approximation (GGA) [36] for exchange and correlation electronic energies and with ultra-soft pseudo-potentials [37]. This method is employed instead of the full-potential linearized augmented plane wave (FLAPW) method because it is more computationally efficient and yet sufficiently accurate, enabling a broader range of atomic structures to be explored. The GGA is expected to be more accurate than the local density approximation (LDA) for interface calculations [38]. To be more specific, the interface calculations are performed on the coherent γ-Ni(111)/Al_2O_3(0001) interface using a $3 \times 3 \times 1$ Monkhorst-Pack [39] (M-P) k-mesh. All calculations are spin-polarized with a high energy-cutoff of 400 eV for the plane-wave basis set. Calculations of the Pt interactions in bulk γ-Ni use a

larger superlattice of 3 × 3 × 3 (fcc) and a 2 × 2 × 2 M-P *k*-mesh. Lattice vibrations are considered within the quasi-harmonic approximation using the direct supercell method. Computational details can be found elsewhere [29]. For simplification, electron–phonon interactions and magnetic contributions are neglected.

Equilibrium pure interfacial structures

For the ensuing interface computations, a sandwich interface model of Ni(111)/Al_2O_3(0001) is employed, with a slab of Al_2O_3 (0001) layers (consisting of six O-layers and 12 Al-layers for the stoichiometric interface (Al terminated), sandwiched between two Ni slabs (each consisting of four Ni (111) atomic layers). Equilibrium interfacial structures (or stoichiometry) must be computed with appropriate means for addressing the lattice constant mismatch. With the current state of the art, it is not possible to have an arbitrarily large unit cell with misfit dislocations included naturally. So we strain the lattices into commensuration. Such straining is compatible with observations of misfit edge dislocations in a related (Nb/α-Al_2O_3) system, whose HRTEM micrograph [40] is shown in Fig. 2. Namely, the dislocation is sufficiently offset from the interface that the in-plane strain in the metal adjacent to the interface is spatially quite uniform and coherent with the oxide. We consider three types of coherent interfaces [32] (Types I, II, and III) which vary in strain and orientation. To be able to compare W_{sep} among different interface types, we ensure that all fully separated surface slabs are subjected to the same imposed strains as in the ensemble interface, so that strain contributions to the energies of surface slabs can be dissociated from W_{sep}. We have found [32] that W_{sep} is substantially more sensitive to interfacial stoichiometry (termination) than upon commensuration strain: W_{sep} for the Al- and O-rich interfaces are four and six times larger than that for the stoichiometric interface, respectively. Following Fig. 2, we obtain commensuration [32] via a tensile strain on Ni(111) of 4.75% and an identical compressive strain on Al_2O_3(0001).

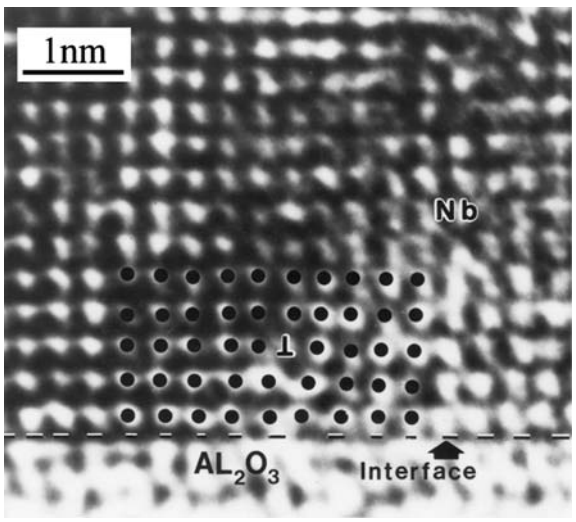

Fig. 2 A HRTEM micrograph [40] of a Nb/α-Al_2O_3 interface at atomic resolution. Note the misfit edge dislocation with a three atomic layer standoff from the interface. The two Nb(111) atomic layers between the misfit dislocation and the α-Al_2O_3(0001) surface exhibit a tensile strain distribution into commensuration

Equilibrium Interfacial Stoichiometry

To determine the appropriate interfacial stoichiometry, we must evaluate the interfacial energy γ_I as [26]:

$$\gamma_I(a_{Al},T) = \frac{1}{2A}\left[G_o - \frac{1}{3}N_O\mu^0_{Al_2O_3} - N_{Ni}\mu^0_{Ni} - (N_{Al} - \frac{2}{3}N_O)\left(\mu^0_{Al} + kT\ln a_{Al}\right)\right], \quad (1)$$

where A is the cross-sectional area of the interface, G_o is the free energy of the interface, and N_i (i = Al, Ni, or O), are the numbers of each type of atom, varying with interfacial stoichiometry. μ^0_{Ni} or μ^0_{Al} is the chemical potential for each pure bulk metal on a per atom basis, and $\mu^0_{Al_2O_3}$ is the chemical potential of Al_2O_3 on the stoichiometric basis. The Al chemical activity $a_{Al} = a_{Al}(x_{Al},T)$ is the value for Al in bulk γ-Ni(Al), where x_{Al} is the atomic percent of Al in the bulk. With the assumption of thermodynamic equilibrium between bulk γ-Ni(Al) and the interface, a_{Al} is also the Al activity in the interface. The interfacial energy γ_I is independent of a_{Al} for stoichiometric interfaces (due to $N_{Al} = \frac{2}{3}N_O$). For each termination, the equilibrium interfacial structure is determined by minimizing γ_I with respect to the atomic coordinates of Ni, Al, and O. We have found [32] with the computed Al activities for $x_{Al} = 1 \rightarrow 15$ at.% for, e.g., T = 1,300 K, that the interface between the thermally grown α-Al_2O_3 and the alloy is Al-rich (Ni/$(Al_2O_3)_{Al2}$), but close to the boundary with the stoichiometric phase (Ni/$(Al_2O_3)_{Al}$). The ensuing calculations with doping/alloying elements and impurities are therefore carried out for both the Al-rich and the stoichiometric phases.

Interfacial segregation and adhesion

To assess the effects of impurities and dopants on adhesion, we first compute the heats of segregation, ΔG_{seg}, from inside the bulk alloy to various interstitial or substitutional sites on the interface. These heats must be exothermic to enable segregation. Comparison of ΔG_{seg}among segregating

elements to the same interface provides the relative ordering of segregation preference. When segregation does occur, we then determine the plane of the separation by finding the minimum W_{sep}, which measures the influence of segregating elements on adhesion.

Interfacial segregation

In the following, we compare in Figs. 3, 4, and 5 the results for Pt obtained here with our earlier results [30, 32] for S and Hf. (i) *For the stoichiometric interface*, at 1/3 monolayer (ML) coverage, Hf segregates to Al-substitutional, interstitial, and Ni substitutional sites, with $\Delta G_{seg} = 1.74$, 1.79, or 1.29 eV/atom, respectively. Results for heats of segregation and works of separation are shown in Fig. 3. While the clean stoichiometric interface has a fairly low W_{sep} that is about one-third of that of the Al-rich interface, we find that Hf can strengthen this interface sufficiently to achieve a W_{sep} as large as that of the Al-rich interface. This is an important benefit of Hf on adhesion of the stoichiometric interface. The alloying element Pt can only segregate to Ni substitutional sites with $\Delta G_{seg} = 0.41$ eV/atom, and it has a relatively small effect on W_{sep}. The impurity S segregates to interstitial sites with $\Delta G_{seg} = 1.55$ and Ni substitutional sites with $\Delta G_{seg} = 1.24$ eV/atom. Substitutional S and especially interstitial S significantly weaken the adhesion of the stoichiometric interface. Recall that a higher ΔG_{seg} corresponds to a more energetically favored segregation site (from the thermodynamics viewpoint), or a more frequently occupied site (from the statistical mechanics viewpoint). At the relatively weakly bonded stoichiometric interface, comparing the heats of Hf and Pt segregation to those of S segregation, we see that segregated Hf can inhibit S segregation to the interface,

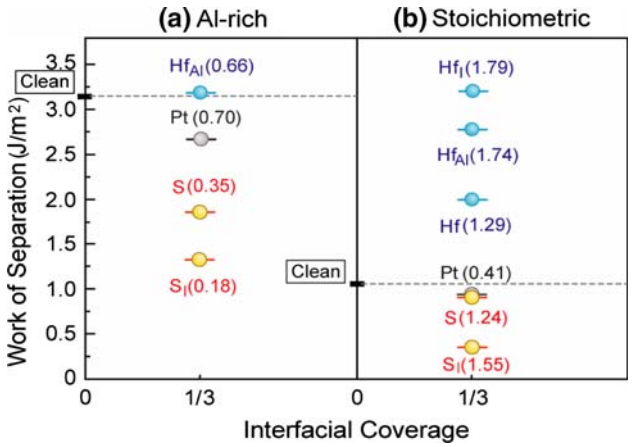

Fig. 3 The work of separation, W_{sep}, as a function of interfacial coverage for (**a**) the Al-rich and (**b**) the stoichiometric interfaces. Here one monolayer (ML) is the number of Ni atoms in a single atomic layer. Values in parentheses are the heats of segregation (in units of eV/atom)

while Pt cannot. We conclude that Hf can inhibit the deleterious interfacial effect of S on adhesion through preferential segregation, while Pt is not beneficial in this regard for this interface. (ii) *For the Al-rich interface*, Hf can only segregate to Al-substitutional sites with $\Delta G_{seg} = 0.66$ eV/atom, and it has a relatively minor effect on W_{sep}. Pt only segregates to Ni substitutional sites, with $\Delta G_{seg} = 0.70$ eV/atom, and a slight lowering of W_{sep}. S segregates to Ni substitutional sites with $\Delta G_{seg} = 0.35$ and to interstitial sites with $\Delta G_{seg} = 0.18$ eV/atom. S significantly weakens the adhesion of the Al-rich interface, as much as on the stoichiometric interface. Note also that S has significantly lower heats of segregation (and thus significantly lower segregation tendencies) to the Al-rich interface than to the stoichiometric interface. Pt, which has the highest heat of segregation, can inhibit S segregation to substitutional sites where site competition takes place (nevertheless these segregations can be kinetic-controlling processes). The W_{sep} for segregated Pt is significantly higher than for segregated S. We also find that interstitial S segregation can be inhibited by segregated Pt at the interface. We hence conclude that Pt can be beneficial for the Al-rich interface by inhibiting S segregation. When the Al-rich interface is predominant, as predicted by our interfacial phase diagram [30, 32], these Pt results are consistent with recent experimental observations [41], where Pt is found to segregate to the γ/γ'-Ni(Al)/Al_2O_3 interface and correspondingly the interfacial S content is lowered and the interfacial strength increased.

Figure 4 provides an atomistic view of our results. The Ni atoms are shown in blue in the top half of the interface, while the α-Al_2O_3 is in the bottom half. Top views of the interfacial layers are shown below each interface. The horizontal dashed lines are annotated with the corresponding W_{sep}. The Al-rich interfaces are shown in Fig. 4a, while the stoichiometric interfaces can be found in Fig. 4b. Note first that the stronger Al-rich interface (clean) has its lowest W_{sep} one atomic layer into the Ni, while the weaker stoichiometric interface (clean) has the weakest (or least strongly bound) atomic plane right at the interface. Figure 5 provides electron density contours for these interfaces. The pure Al-rich interface is found in Fig. 5a, while the stoichiometric interfacial results are in Fig. 5b. Figure 5a indicates some metallic character in the bonding between Ni and the Al-rich α-Al_2O_3 surface. Figure 5b suggests a directed partially ionic, partially covalent bond between Ni and O atoms across the clean stoichiometric interface. When segregation does occur, we compute W_{sep} over different interlayer planes and search for the minimum W_{sep} that results from the weakest interfacial bonding. (i) *S segregation.* Although it has a lower segregation tendency to the Al-rich interface (due to the smaller heats of segregation), the strong deleterious effects of S are evident on

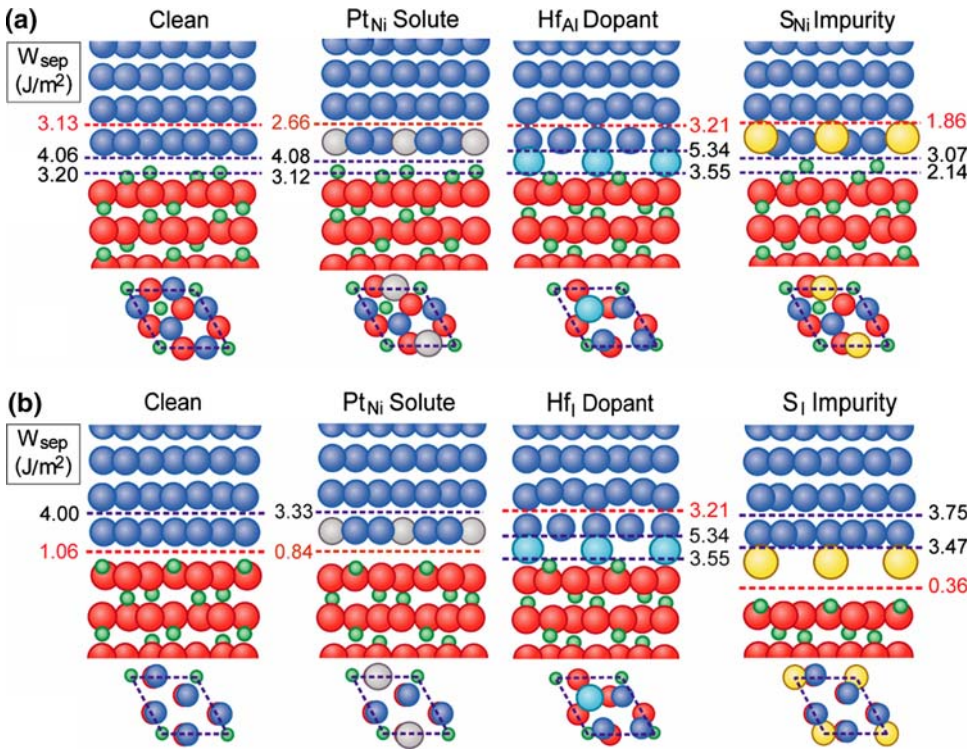

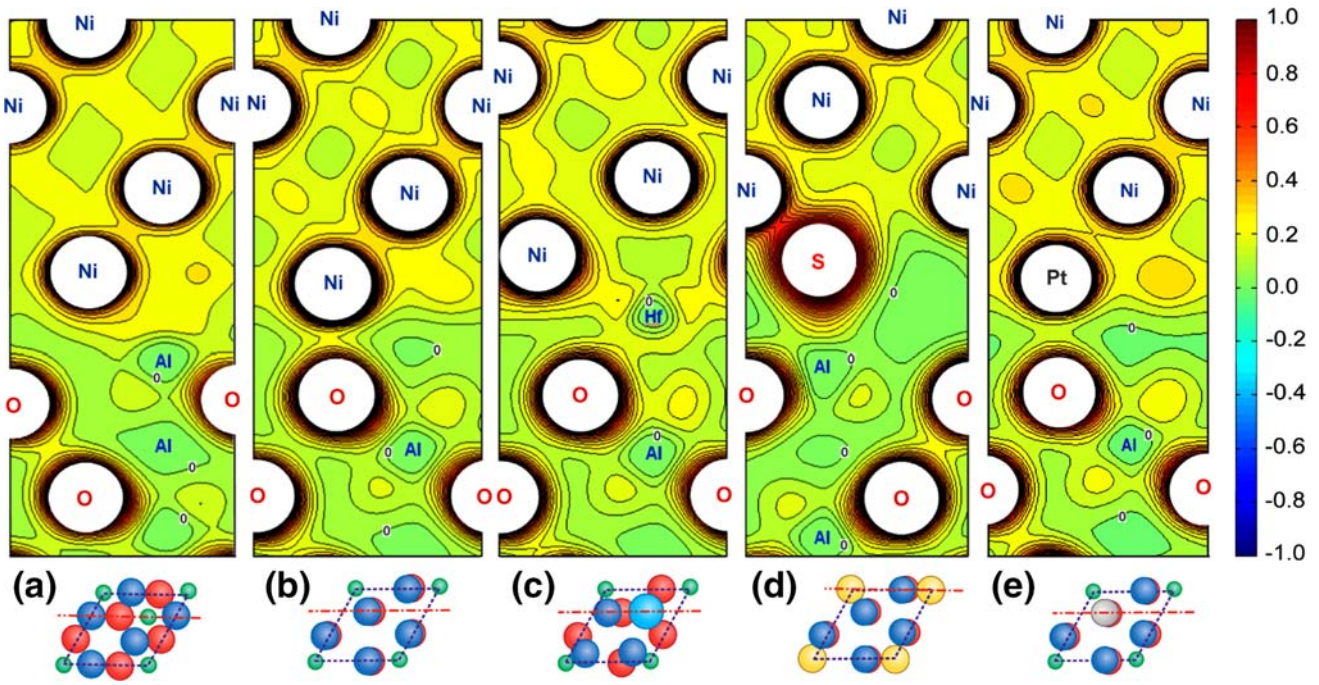

Fig. 4 W_{sep} for (**a**) the Al-rich and (**b**) the stoichiometric interfaces shown with and without segregants. Corresponding top-views of interfacial layers are shown at the bottom. Ni, Al, O, Pt, Hf, and S are represented in dark blue, green, red, silver, light blue, and yellow, respectively

Fig. 5 Electron density contours (in unit of e/Å^3). **a** The clean Al-rich interface showing the metallic bonding between the Ni and the extra Al. **b** The clean stoichiometric interface showing the Ni–O bonds with each Ni atop each O. **c** The stoichiometric interface containing segregated Hf (Hf_I) shown on the same plane as (**b**). Note the Hf knitting the interface together via bonds with both Ni and O. **d** The stoichiometric interface containing segregated S (S_I). Note the S pushes the Ni and O apart, weakening that bond, and a relatively weak S–Al bond is created. **e** The stoichiometric interface containing segregated Pt shown on the same plane as (**b**). Note the new Pt–O bond is weaker than the previous Ni–O bond. The dash-dot lines at the bottom correspond to the positions of the contour planes in top-views

both interfaces, as shown graphically in Figs. 4 and 5. S segregation to an interstitial site in the stoichiometric interface at 1/3 ML coverage (one S per surface unit cell) has a relatively large effect on W_{sep}, as exhibited by the increased separation between the Ni and α-Al_2O_3 surfaces. (ii) *Hf segregation.* At the relatively strong Al-rich

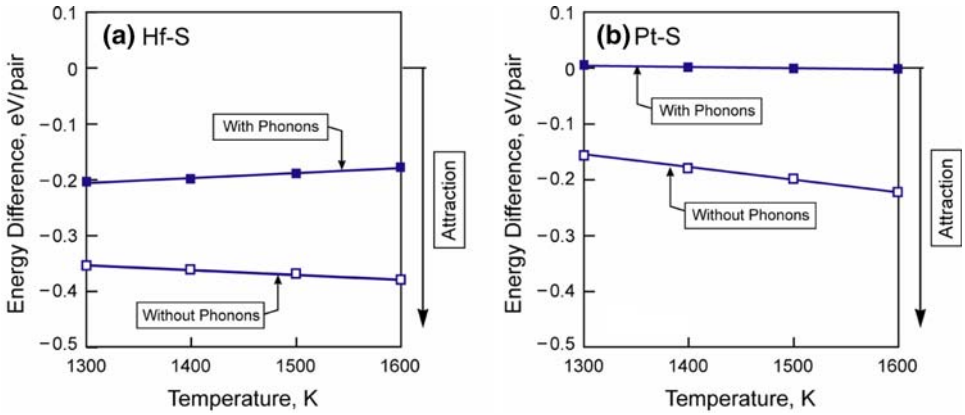

Fig. 6 Interaction energies of Hf–S and Pt–S in bulk γ-Ni as a function of temperature, without and with phonons

interface, Hf segregates to Al-substitutional sites, and the high W_{sep} remains almost unaffected, see, Figs. 3a and 4a. The separation now occurs inside the Ni, between the first and second Ni atomic layers, for both the clean and Hf-segregated Al-rich interfaces. At the relative weak stoichiometric interface, Hf benefits are pronounced, with W_{sep} being increased by about a factor of 3. Figure 4 shows that for Hf substituting for Al at 1/3 ML, the Al-rich and stoichiometric interfaces become identical, with correspondingly identical W_{sep}. It is quite unusual for a segregant to increase W_{sep} so substantially. Electron density contours, Fig. 5c, affirm that Hf bonds to Ni and O atoms across the interface. While there is some strain due to the introduction of Hf (the Ni and O interfacial layers separate slightly), the bonding between those two layers is sufficiently strengthened by the Hf so that the weakest link now appears within the Ni. (ii) *Pt segregation* to Ni substitutional sites at both interfaces reduces W_{sep} by 15–20%. This happens because the newly formed interfacial Pt–O bonds, Fig. 5e, are slightly weaker than the Ni–O bonds of the pure interface, Fig. 5b. At the Al-rich interface, Pt segregation occurs in preference to S and can mitigate the deleterious sulfur effect.

We can now summarize the comparison between Hf and Pt effects on adhesion. We find rather different results for the stoichiometric and Al-rich interfaces. For the stoichiometric interface, Pt can neither block S segregation nor directly increase W_{sep} through enhanced interfacial bonding, while Hf both inhibits S segregation and strongly increases interfacial bonding. On the other hand, for the Al-rich interface, Pt does tend to block S segregation, as does Hf. Neither Hf nor Pt has a substantial direct effect on W_{sep} for the Al-rich interface.

Gettering sulfur in bulk γ-Ni

We have shown earlier the strong deleterious sulfur effects: S can segregate to both interface types, and weaken the adhesion by, e.g., 60–70%. Such weak bonding regions resulting from S attacks may act as the origin of a crack or the preferential path of the cracks under stresses. For this reason, the S-content in modern, commercial alloys has been reduced to the level of no more than tens of ppm (by desulfurization processes such as hydrogen-based annealing). Historically, RE-dopants have been introduced for the purpose of reacting with and tying up S in the bulk metal alloy, due to their strong sulfide forming ability, preventing S from segregating to the interface. We have also shown earlier [30, 32] that Hf can indeed tie up S in bulk γ-Ni (results are plotted in Fig. 6a), inclusive of the temperature dependences of the enthalpies and entropies within the quasi-harmonic approximation as described in Ref. [29]. The resulting free energies calculated for atom pairs were compared at the first nearest-neighbor (NN) distance of 2.5 Å and at a larger separation of ~8.5 Å (5th NN)—the latter was chosen to be sufficiently large that the two atoms are essentially non-interacting. The difference in these energies indicates the strength and sign of the interaction. As seen in Fig. 6a, even though vibrational energies weaken the bond, Hf binds S in bulk γ-Ni at all realistic temperatures. Figure 6b represents results for Pt interacting with S. The binding of Pt–S is significantly weaker than Hf–S, and thermal vibrations/phonons set S free from Pt for potential interfacial segregation. We therefore conclude that the benefits of Hf also include the strong gettering efficiency for deleterious S in bulk γ-Ni. This mechanism is, however, not viable for Pt. The experimental study [41] on the γ/γ'-Ni(Al)/Al_2O_3 interface also suggests that adding Hf can virtually eliminate S from the interface, while Pt lowers the interfacial S coverage but does not eliminate it.

Conclusions

Developing improved TBC systems with high durability requires that all major factors affecting the adhesion of the γ-Ni(Al)/α-Al_2O_3 interface be well understood. In this

article, we have reviewed basic understanding of the interrelations of structure, composition and adhesion developed from first-principles DFT. Pt effects on the adhesion through interfacial stoichiometry, segregation, and interface bonding have been discussed in terms of the interfacial work of separation, and compared with those of Hf and S. The following specific findings have been substantiated:

(i) *Interfacial stoichiometry* strongly affects the adhesion: the Al-rich interface has a significantly larger W_{sep} (by a factor of 3) than its stoichiometric counterpart, and the O-rich interface can be even stronger.

(ii) *The Al activity* in γ-Ni(Al) has been determined, inclusive of the vibrational and thermal electronic contributions to enthalpy and entropy. Together with the interfacial "phase diagram" calculations, it is concluded that the most relevant interfacial structures are the Al-rich and stoichiometric phases.

(iii) *Heats of segregation* calculations suggest that Hf, Pt, and S can all segregate to both interfacial phases.

(iv) *S segregation* to the interface can degrade the adhesion by up to 60–70%. Its detrimental effects can be substantially alleviated by site competition with segregated Hf (at both interfaces) and Pt (at the Al-rich interface).

(v) *Hf segregation* has minimal effects at the Al-rich interface, but dramatically increases W_{sep} (by a factor 3) for the stoichiometric interface, equalizing the adhesion of both interfacial phases. The electron density contours reveal that this benefit is attributed to its direct contribution to interfacial bonding, where Hf effectively knits the two surfaces together via, e.g., bonding to Ni and across the interface to O. Hf also alleviates S segregation by site competition at both the stoichiometric and Al-rich interfaces.

(vi) *Pt segregation* cannot directly promote interfacial bonding, but it can retain a relative strong adhesion by significantly alleviating S segregation via site competition to the Al-rich interface.

(vii) *Doping with Hf* can efficiently getter S in bulk γ-Ni, therefore effectively inhibiting the deleterious S segregation, while Pt cannot.

Acknowledgements The authors are grateful for Air Force Office of Scientific Research (AFOSR) support from Grant No.FA9550-05-C-0039 and many helpful discussions with X.-G. Wang and W. Zhang. We gratefully acknowledge the HRTEM micrograph of Fig. 2 sent to us by Rühle M. (See [40]).

References

1. Evans AG, Mumm DR, Hutchinson JW, Meier GH, Pettit FS (2001) Prog Mater Sci 46:505
2. Mumm DR, Evans AG (2000) Acta Mater 48:1815
3. Evans AG, Clarke DR, Levi CG (2008) J Euro Ceram Soc 28:1405
4. Funkenbusch AW, Smeggil JG, Bornstein NS (1985) Metall Trans A 16:1164
5. Smeggil JG, Funkenbusch AW, Bornstein NS (1986) Metall Trans A 17:923
6. Smialek JL, Jayne DT, Schaeffer JC, Murphy WH (1994) Thin Solid Films 235:285
7. Smialek JL (2000) JOM 52:22
8. Hou PY (2000) J Mater Sci Lett 19:577
9. Smialek JL (1987) Metall Trans Commun 18A:164
10. Khanna AS, Wasserfuhr C, Quadakkers WJ, Nickel H (1989) Mater Sci Eng A 120:185
11. Meier GH, Pettit FS, Smialek JL (1995) Mater Corros 46:232
12. Hou PY (1999) Oxid Met 52:337
13. Haynes JA, Pint BA, More KL, Zhang Y, Wright IG (2002) Oxid Met 58:513
14. Gleeson B (2006) J Propul Power 22:375
15. Haynes JA, Zhang Y, Lee WY, Pint BA, Wright IG, Cooley KM (1999) Elevated Temp Coat Sci Technol III 3:185
16. Zhang Y, Lee WY, Haynes JA, Wright IG, Pint BA, Cooley KM, Liaw PK (1999) Metall Mater Trans 30A:2679
17. Cadoret Y, Bacos M-P, Josso P, Maurice V, Marcus P, Zanna S (2004) Mater Sci Forum 461–464:247
18. Bouchet R, Mevrel R (2003) Calphad 27:295
19. Cadoret Y, Monceau D, Bacos M-P, Josso P, Maurice V, Marcus P (2005) Oxid Met 64:185
20. Meier GH, Pettit FS (1989) Surf Coat Technol 39:1
21. Niu Y, Wu WT, Boone DH, Smith JS, Zhang JQ, Zhen CL (1993) J Phys 3:511
22. Angenete J, Stiller K, Langer V (2003) Oxid Met 60:47
23. Tawancy HM, Sridhar N, Abbas NM, Rickerby D (1995) Scripta Mater 33:1431
24. Das DK, Roy M, Singh V, Joshi SV (1999) Mater Sci Technol 15:1199
25. Fountain JG, Golightly FA, Stott FH, Wood GC (1976) Oxid Met 10:341
26. Zhang W, Smith JR, Evans AG (2002) Acta Mater 50:3803
27. Saiz E, Cannon RM, Tomsia AP (1999) Acta Mater 47:4209
28. Wang X-G, Smith JR, Evans AG (2006) Phys Rev B 74:081403
29. Jiang Y, Smith JR, Evans AG (2006) Phys Rev B 74:224110
30. Jiang Y, Smith JR, Evans AG (2008) Appl Phys Lett 92:141918
31. Zhang W, Smith JR, Evans AG (2003) Phys Rev B 67:245414
32. Smith JR, Jiang Y, Evans AG (2007) Int J Mater Res (Z Metallkd) 98:1214
33. Dehm G, Rühle M, Ding G, Raj R (1995) Philos Mag B 71:1111
34. Kresse G, Hafner J (1993) Phys Rev B 47:558
35. Kresse G, Furthmüller J (1996) Phys Rev B 54:11169
36. Perdew JP, Wang Y (1992) Phys Rev B 45:13244
37. Vanderbilt D (1990) Phys Rev B 41:7892
38. Smith JR, Zhang W (2000) Acta Mater 48:4395
39. Monkhorst HJ, Pack JD (1976) Phys Rev B 13:5188
40. Gutekunst G, Mayer J, Rühle M (1994) Scripta Metall Mater 31:1097
41. Hou P (2008) Annu Rev Mater Res 38:275